Available online at www.sciencedirect.com
SCIENCE DIRECT®
Journal of Nuclear Materials 352 (2006) 309–317
journal of nuclear materials
www.elsevier.com/locate/jnucmat

Evaluation of thermal conductivity of zirconia-based inert matrix fuel by molecular dynamics simulation

T. Arima [a,*], S. Yamasaki [a], K. Yamahira [a], K. Idemitsu [a], Y. Inagaki [a], C. Degueldre [b]

[a] Institute of Environmental Systems, Faculty of Engineering, Kyushu University, 6-10-1 Hakozaki, Fukuoka 812-8581, Japan
[b] Laboratory for Material Behaviour, Paul Scherrer Institute, 5232 Villigen PSI, Switzerland

Abstract

Molecular dynamics (MD) simulations were performed using Born–Mayer–Huggins interatomic potentials with partially ionic model in order to evaluate the thermal conductivity of zirconia-based inert matrix fuel (IMF). The thermal conductivity was calculated at the equilibrium condition based on Green–Kubo theory and phenomenological equations. For $Er_xY_yM_zZr_{1-x-y-z}O_{2-(x+y)/2}$ (where M = Ce or Pu), the thermal conductivity decreased with increase of y because of the presence of oxygen vacancies as the thermal resistance. It also slightly decreased with increase of z and temperature. However, significant difference could not be found in the thermal conductivity between Ce- and Pu-doped zirconia. The MD thermal conductivity of IMF was in good agreement with the literature data. Concerning the phenomenological coefficients, the cross-coupling effect between energy and charge fluxes was clearly observed at low z value and high temperatures for such zirconia systems.

PACS: 71.15.Pd; 28.41.Bm; 44.10.+i

1. Introduction

Zirconia-based inert matrix fuel (IMF) has been extensively developed as an attractive nuclear fuel in order to burn excess plutonium from nuclear weapons and spent fuels due to its advantages for utilization of Pu as nuclear fuel, e.g., high melting point, phase stability, stability against irradiation, etc. [1]. Although it is known to have a low thermal conductivity [2], CERCER (ceramic–ceramic) or CERMET (ceramic–metal) designs can overcome this disadvantage [3].

So far, for zirconia-based IMF, $Er_xY_yPu_zZr_{1-x-y-z}O_{2-(x+y)/2}$ ($x + y = \sim 0.15$), various physico-chemical properties have been investigated by both experimental and simulation methods [2,4–9]. Since thermal conductivity is one of the most important parameters for a nuclear fuel, it must be carefully evaluated by different approaches. In our previous study [9], molecular dynamics (MD) simulations of zirconia-based IMF were performed to evaluate the lattice structure and specific heat but not the thermal conductivity. Therefore, in the

* Corresponding author. Tel.: +81 92 642 3779; fax: +81 92 642 3800.
E-mail address: arimatne@mbox.nc.kyushu-u.ac.jp (T. Arima).

0022-3115/$ - see front matter © 2006 Elsevier B.V. All rights reserved.
doi:10.1016/j.jnucmat.2006.02.066

present MD study, the thermal conductivity of zirconia-based IMF is discussed in terms of composition and temperature.

Thermal conductivity of nuclear fuels, e.g., UO_2, PuO_2, UO_2–PuO_2 solid solution, has already been studied by MD simulations [10–14]. In many cases, MD simulations were performed under an equilibrium condition, so-called 'EMD' simulation, and the thermal conductivity was calculated using Green–Kubo formulation [10–13]. Lindan and Gillan obtained the thermal conductivity of UO_2 by Green–Kubo relation and phenomenological equations expressed by transport coefficients and fluxes [13]. Non-equilibrium MD (NEMD) simulations were performed for UO_2 by Motoyama [14]. On the other hand, for stabilized zirconia such as ZrO_2–Y_2O_3, the crystal structure, ionic diffusion, and specific heat have been studied by MD techniques [15–24]. However, there was little literature in which the thermal conductivity of stabilized zirconia was discussed. Schelling performed NEMD for the ZrO_2–Y_2O_3 system [23], and the thermal conductivity was a little overestimated.

In the present study, the thermal conductivity of $Er_xY_yM_zZr_{1-x-y-z}O_{2-(x+y)/2}$ (where $x = 0.05$, $y = 0.1$, $z = 0.0$–0.2, M = Ce or Pu) has been calculated between 300 and 2000 K. EMD simulations were performed with Born–Mayer–Huggins interatomic potentials, and the thermal conductivity was deduced based on Green–Kubo theory. Furthermore, phenomenological equations were considered for calculation of thermal conductivity because it was expected that heat and charge fluxes were strongly coupled at high temperatures.

2. Equilibrium molecular dynamics simulation

2.1. Interatomic potential with fully or partially ionic model

The EMD program MXDORTO developed by Kawamura [25] was used to obtain thermal properties of stabilized zirconia. So far, it has been assumed that such zirconia is the fully ionic crystal in which ionic charges of Zr and O ions are +4 and −2, respectively. So that the thermal expansion for the fully ionic model (FIM) was a little smaller than experimental data in our previous study [24]. Such a trend was observed especially for high temperatures ($T > \sim 1000$ K). The partially ionic model (PIM) was introduced as the alternative to FIM in order to reduce the ionic bonding effect.

With the FIM, the Born–Mayer–Huggins (BMH) interatomic potential, which is widely used for the simulation of ionic materials, is written by

$$U_{\mathrm{FIM}}(r_{ij}) = \frac{z_i z_j e^2}{r_{ij}} + A_{ij}\exp\left(-\frac{r_{ij}}{\rho_{ij}}\right) - \frac{C_{ij}}{r_{ij}^6}, \tag{1}$$

where r_{ij} is the distance between ions of types i and j, z_i is the charge of type i, and A_{ij}, ρ_{ij} and C_{ij} are called potential parameters which depend on the combination of two types of ions. On the other hand, the BMH potential with PIM is given by

$$U_{\mathrm{PIM}}(r_{ij}) = \frac{z_i z_j e^2}{r_{ij}} + f_0(b_i + b_j) \times \exp\left\{\frac{(a_i + a_j - r_{ij})}{(b_i + b_j)}\right\} - \frac{c_i c_j}{r_{ij}^6}, \tag{2}$$

where f_0 is the adjustable parameter. Potential parameters, a_i, b_i and c_i, are given to the ion of types i. The first term of the right side of Eqs. (1) and (2) stands for the Coulomb interaction, the second one is the repulsive potential between ionic cores, and the third one originates from the van der Waals interaction. Concerning the long-range Coulomb interaction, Ewald summation was considered in the MXDORTO program. For the PIM, the ionic bonding of 67.5% is assumed [26–28], e.g., $z_{\mathrm{Zr}} = +2.70$.

Potential parameters for the FIM were presented in our previous study [9] and the literature [15,29]. For the PIM, potential parameters of Zr and Er ions were determined in the present study, and those of O, Y, Ce and Pu ions were obtained from Refs. [26–28]. Concerning the Zr ion, we refer to the thermal expansion of yttria-stabilized zirconia, $Y_{0.148}Zr_{0.852}O_{1.926}$ (i.e., 8 mol%Y_2O_3). Because pure ZrO_2 has three different crystal structures, monoclinic, tetragonal and cubic, under atmospheric pressure, we could not obtain the potential parameters to satisfy these different phases. Potential parameters of Er ion were determined based on the thermal expansion of Er_2O_3. The BMH potential parameters used for FIM and PIM are summarized in Tables 1 and 2, respectively.

2.2. Formalization of thermal conductivity based on Green–Kubo theory and phenomenological equations

In the present study, EMD simulations were performed for the stabilized zirconia system, which was considered as a superionic conductor. Early studies

Table 1
Potential parameters of BMH interatomic potential with FIM

Interaction	A_{ij} (kJ mol^{-1})	ρ_{ij} (nm)	C_{ij} (kJ nm^6 mol^{-1})	Source
Er–O	12.780×10^4	0.03492	0.0	[9]
Y–O	12.978×10^4	0.03491	0.0	[29]
Ce–O	11.350×10^4	0.03810	0.0	[9]
Pu–O	10.900×10^4	0.03830	0.0	[9]
Zr–O	9.512×10^4	0.03760	0.0	[15]
O–O	21.960×10^5	0.01490	2.691×10^{-3}	[15]

Table 2
Potential parameters of BMH interatomic potential with PIM

Ion	z_i	a_i (nm)	b_i (nm)	c_i (J$^{-0.5}$ nm^3 mol$^{-0.5}$)	Source
Er	2.025	0.11031	0.00129	0.0	Present study
Y	2.025	0.11200	0.00130	0.0	[27]
Ce	2.70	0.13300	0.00454	0.0	[26]
Pu	2.70	0.12720	0.00325	0.0	[28]
Zr	2.70	0.10950	0.00254	0.0	Present study
O	−1.35	0.18470	0.01660	1.294	[26]

of binary ionic systems (e.g., NaCl, KCl, CaF_2, UO_2, etc.) discussed the thermal conductivity based on the phenomenological equations and cross-effects expressed by macroscopic fluxes and forces [13,30–33]. According to the literature [13,32,33], fluxes of charge and energy, $\vec{J}_Z$ and $\vec{J}_E$, are considered into linear phenomenological relations as alternative fluxes of charge and heat. These phenomenological transport equations describe the vectorial phenomena of charge current, energy conduction, and their cross-effects:

$$\vec{J}_Z = -L_{ZZ}T\nabla\left(\frac{\mu_Z}{T}\right) - L_{ZE}T\nabla(T), \tag{3}$$

$$\vec{J}_E = -L_{EZ}T^2\nabla\left(\frac{\mu_Z}{T}\right) - L_{EE}\nabla(T). \tag{4}$$

In the right sides of the above equations, each term consists of the phenomenological coefficient L and corresponding thermodynamic force. Here, μ_Z is the electrochemical potential, which is relating to chemical potential, electric potential, and partial enthalpy. Applying the Onsager reciprocal relation, $L_{ZE} = L_{EZ}$, the thermal conductivity κ can be expressed by

$$\kappa = L_{EE} - \frac{L_{EZ}^2}{L_{ZZ}}\cdot T. \tag{5}$$

The Green–Kubo theory gives transport coefficients in Eq. (5) for EMD calculations as time-integrals of auto-correlation functions of microscopic fluxes:

$$L_{\alpha\beta} = \frac{1}{V}\int_0^\infty \mathrm{d}t C_{\alpha\beta}(t), \tag{6}$$

where V is the cell volume simulated. Each correlation function $C_{\alpha\beta}$ (α, $\beta = Z$, E) for the combination of α and β can be defined under thermal equilibrium condition as follows:

$$C_{ZZ}(t) = \frac{1}{3k_BT}\left\langle \vec{j}_Z(t)\cdot\vec{j}_Z(0)\right\rangle, \tag{7}$$

$$C_{EZ}(t) = \frac{1}{3k_BT^2}\left\langle \vec{j}_E(t)\cdot\vec{j}_Z(0)\right\rangle, \tag{8}$$

$$C_{EE}(t) = \frac{1}{3k_BT^2}\left\langle \vec{j}_E(t)\cdot\vec{j}_E(0)\right\rangle, \tag{9}$$

where k_B is the Boltzmann constant, $\vec{j}_Z(t)$ and $\vec{j}_E(t)$ are the charge and energy fluxes, respectively. These microscopic fluxes can be expressed by following equations:

$$\vec{j}_Z(t) = \sum_{i=1}^{N} z_i e\vec{v}_i, \tag{10}$$

$$\vec{j}_E(t) = \sum_{i=1}^{N}\left[\frac{m_i v_i^2}{2} + \frac{1}{2}\sum_{j\neq i}U(r_{ij})\right]\vec{v}_i + \frac{1}{2}\sum_{i=1}^{N}\vec{v}_i\cdot\vec{r}_{ij}\vec{F}_{ij}, \tag{11}$$

where m_i is the mass of ith particle, v_i the velocity. According to the above interpretation of the phenomenological equations, the thermal conductivity finally can be evaluated in Eq. (5) by the EMD simulations. The term of $\vec{r}_{ij}\vec{F}_{ij}$ in Eq. (11) corresponds to the tensor $\overleftrightarrow{S}_i$ given by Motoyama [14]. It is introduced to avoid divergences arising from the long range of Coulomb interactions based on the model given for the one-component plasma [34], and of course allows for the short-range potentials. When the Coulomb interaction includes the interatomic potential, the definition of energy fluxes is not as simple as in the case of the Lennard–Jones potential. In the present study, the calculation algorithm of thermal conductivity was added to the MXDORTO code according to the formulation described by Motoyama [14].

2.3. EMD simulation procedure

For $Er_xY_yM_zZr_{1-x-y-z}O_{2-(x+y)/2}$ (M = Ce or Pu), MD simulations were performed according to the following procedure. The Zr^{4+} and O^{2-} ions were arranged at each regular site of the fluorite structure. The trivalent ions (Y^{3+} and Er^{3+}) and oxygen vacancies were substituted at random on Zr and O regular

sites, respectively. The number of oxygen vacancies was equivalent to half the total number of trivalent ions because of the requirement of electrical neutrality. Simultaneously, Ce^{4+} (or Pu^{4+}) ions were arranged at random on Zr sites. In order to equilibrate the simulated system for desired temperature and pressure, the so-called 'initial relaxation' calculation was done for 2×10^4 steps (=40 ps). Then, the EMD simulation with 2×10^4 steps was performed to obtain the relevant results under the desired condition. Lattice constants were obtained in the *NPT* ensemble. In order to obtain reliable results of thermal conductivity, three or five runs of 5×10^5 steps were needed and the calculations were performed in the microcanonical ensemble (N,V,E). Simulated systems composed $3 \times 3 \times 3$ fluorite unit cells (max. 324 ions) were considered. Considering the CPU time consumption and the statistics, NEMD simulation may be suitable for calculation of the thermal conductivity rather than EMD. However, this study is the first step for us to evaluate the thermal conductivity by the MD simulation.

3. Results and discussion

3.1. Thermal expansion of inert matrix fuel

According to previous crystallographic studies of $Er_xY_yM_zZr_{1-x-y-z}O_{2-(x+y)/2}$ (M = Ce or Pu) [5,6,35], it is known that zirconia-based IMF has the fluorite-type cubic phase for $z = 0.0$–0.2 and $x + y = \sim 0.15$. This was also shown in our previous MD study [9]. Here, the lattice constants were obtained as a function of temperature by both FIM and PIM models for MD simulations. In addition, the lattice constant of Ce-doped zirconia made through sol–gel route was experimentally determined by high temperature X-ray diffraction (HTXRD) measurements. The results of thermal expansion of Ce- and Pu-doped IMFs are given to Fig. 1(a) and (b), respectively. As shown in Fig. 1(a), the difference between MD and HTXRD is smaller for PIM than for FIM due to the reduced ionic character of the valence in the PIM. The same tendency for a larger thermal expansion with the

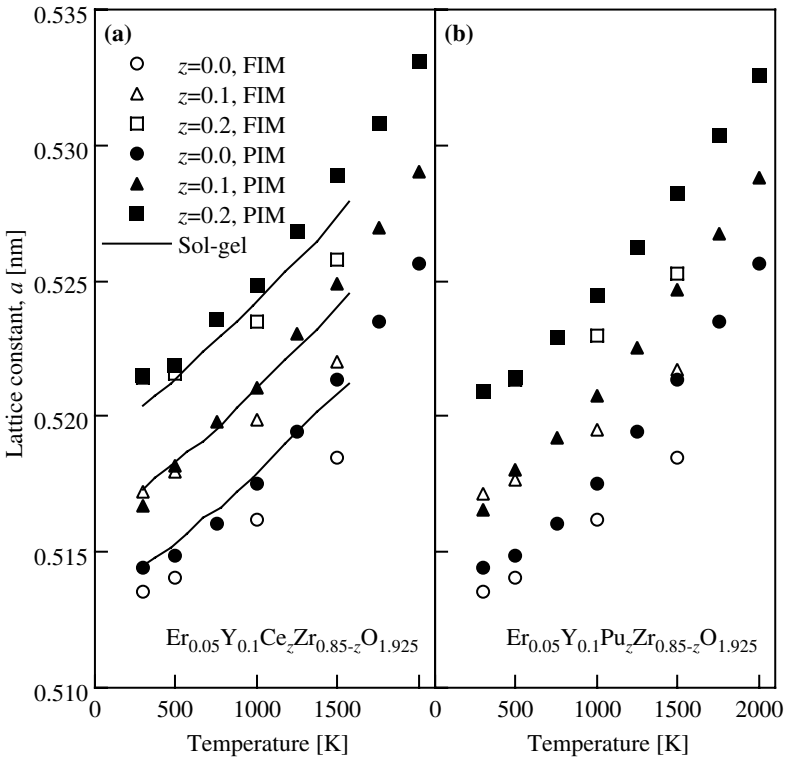

Fig. 1. Thermal expansion of (a) $Er_{0.05}Y_{0.10}Ce_zZr_{0.85-z}O_{1.925}$ and (b) $Er_{0.05}Y_{0.10}Pu_zZr_{0.85-z}O_{1.925}$. FIM and PIM stand for fully and partially ionic models, respectively. Experimental data of Ce-doped zirconia made through sol–gel route was taken by high temperature X-ray diffraction measurement.

PIM than with the FIM is also shown for Pu-doped zirconia (Fig. 1(b)).

3.2. Transport coefficients evaluated by Green–Kubo relation

It is shown in Section 2.2 that each transport coefficient is given by an integral of the auto-correlation function (ACF) of the corresponding fluxes. For $Er_{0.05}Y_{0.1}Pu_zZr_{0.85-z}O_{1.925}$ ($z = 0.0$ and 0.2) at temperatures of 1000 and 2000 K, ACFs and their integrals of energy, charge, and coupling fluxes are plotted as a function of time in Fig. 2. Here, the ACFs are plotted normalized NAFC to the value of ACF at 0.0 ps. At 1000 K, the NACFs approach to almost zero within ~0.5 ps. Simultaneously, each transport coefficient approaches its final value. L_{EE} with $z = 0.2$ seems to be a little smaller than that with $z = 0.0$. The L_{EZ}s show almost equivalent behaviour approaching zero, which indicates weak coupling between energy and charge currents at this temperature. L_{ZZ} decreases with Pu doping. For $Er_{0.05}Y_{0.1}Pu_{0.2}Zr_{0.65}O_{1.925}$, the relaxation time is about 0.3 ps at 2000 K for the NACFs. L_{EE} at 2000 K seems to be a little larger than at 1000 K. L_{EZ} apparently shows a negative value at 2000 K, which suggests

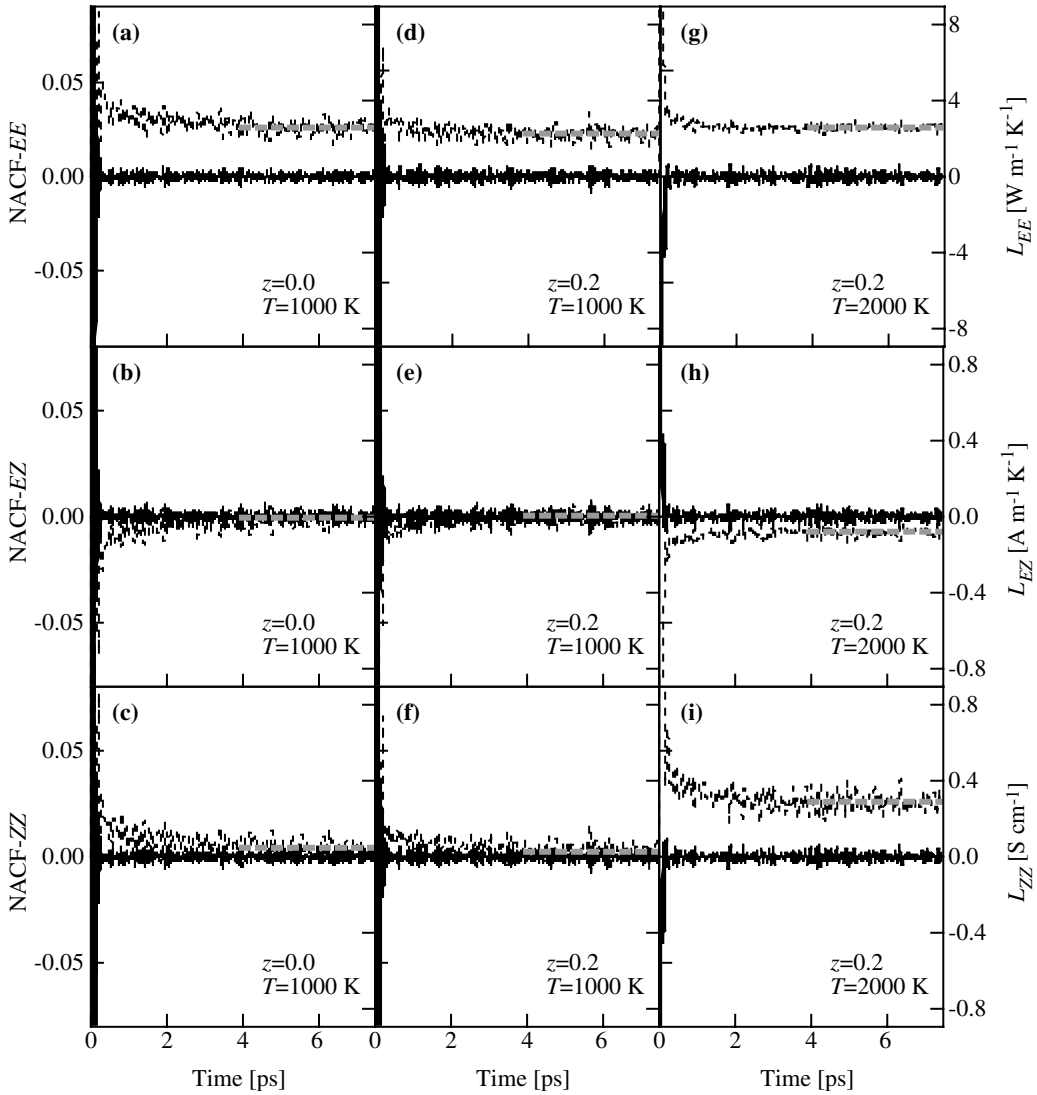

Fig. 2. Normalized auto-correlation function (NACF) and transport coefficient $L_{\alpha\beta}$ (α, $\beta = E$, Z) of $Er_{0.05}Y_{0.10}Pu_zZr_{0.85-z}O_{1.925}$ as a function of time. NACF is proportional to ACF. Solid and dotted line show NACF and $L_{\alpha\beta}$, respectively. Lateral gray dotted line indicates the value finally obtained for $L_{\alpha\beta}$.

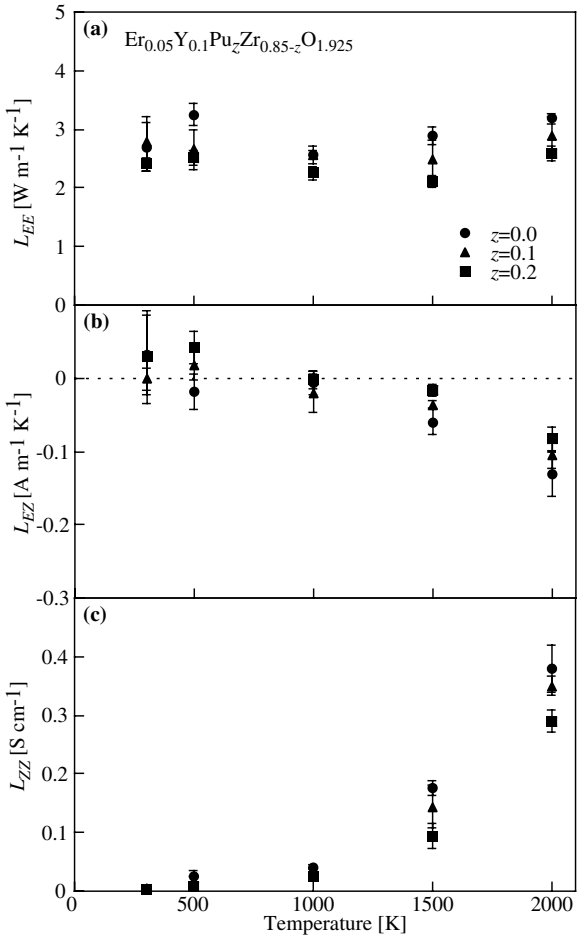

Fig. 3. Transport coefficient $L_{\alpha\beta}$ (α, $\beta = E$, Z) of $Er_{0.05}Y_{0.10}$-$Pu_zZr_{0.85-z}O_{1.925}$ as a function of temperature.

the cross-coupling effect becomes stronger at such higher temperatures. This result is supported by the observation that L_{ZZ} significantly increases at 2000 K. The temperature dependence of the transport coefficients are summarized in Fig. 3. According to the results in Fig. 3(a), L_{EE} seems to be almost constant as a function of temperature. In Fig. 3(b), L_{EZ} remains at almost zero at temperatures less than 1000 K, whereas it takes on a large negative value at temperatures $\geqslant$1000 K. L_{ZZ} exponentially increases with temperature (Fig. 3(c)). On the other hand, the effect of Pu content on the significance of the transport coefficients is lower at higher z values.

3.3. MD thermal conductivity of yttria-stabilized zirconia and IMF

The thermal conductivity obtained by EMD simulation for yttria-stabilized zirconia, $Y_yZr_{1-y}O_{2-y/2}$ ($y = 0.148$, 0.185) is shown in Fig. 4. In this figure, the results from NEMD simulation for a heterogeneous system [23] and experimental data for single crystal $Y_{0.179}Zr_{0.821}O_{1.9105}$ [36] are also plotted. For our EMD simulations, the thermal conductivity is calculated by Eq. (5), including the cross-coupling effect between energy and charge currents. The present EMD result shows that the thermal conductivity slightly decreases with increase in temperature. A similar trend was shown for NEMD [23] and experimental results [36]. Thermal conductivity of polycrystalline stabilized zirconia (cubic, 15 wt% Y_2O_3) was measured by Raghavan [37] and was determined to be $\sim$2.4 W m^{-1} K^{-1} at $T \leqslant 1073$ K. MD calculation gives a little higher thermal conductivity for ZrO_2–Y_2O_3 system. In addition, Fig. 4 clearly shows that the thermal conductivity decreases with increasing y (i.e., Y content). This is the reason why the amount of oxygen vacancies increases with Y doping so that such defects may play the role as the thermal resistance.

Thermal conductivities of $Er_{0.05}Y_{0.1}Ce_zZr_{0.85-z}$-$O_{1.925}$ are plotted in Fig. 5. This figure also includes experimental data of $Er_{0.07}Y_{0.1}Ce_{0.15}Zr_{0.68}O_{1.915}$ [2,8], which are corrected for porosity. The present EMD result shows that the thermal conductivity of $Er_{0.05}Y_{0.1}Ce_zZr_{0.85-z}O_{1.925}$ decreases a little with increase in temperature and Ce content, z. On the other hand, some experimental results show a contradictory trend in the temperature dependence. This may be attributed to the difference in the fabrication process. However, the MD thermal conductivity of Ce-doped zirconia is relatively in good agreement with experimental data between 2.0 and 3.0 W m^{-1} K^{-1}.

Fig. 6 shows the thermal conductivity of $Er_{0.05}$-$Y_{0.1}Pu_zZr_{0.85-z}O_{1.925}$. The present EMD result of Pu-doped zirconia shows a similar trend with Ce-doped zirconia for temperature and z value. In addition, it is in good agreement with experimental data [2]. In Fig. 6, the thermal conductivity obtained by EMD simulation for PuO_2, which has the fluorite crystal structure and no oxygen vacancies, is also plotted [28]. While the thermal conductivity of PuO_2 is inversely proportional to temperature, that of Pu-doped IMF is little dependent on temperature. However, the thermal conductivity of IMF seems to be comparable with that of PuO_2 at higher temperatures. This results from that phonon scattering due to Umklapp process (i.e., intrinsic thermal resistance) dominates at such temperatures. On the other hand, the contribution of oxygen vacancies introduced

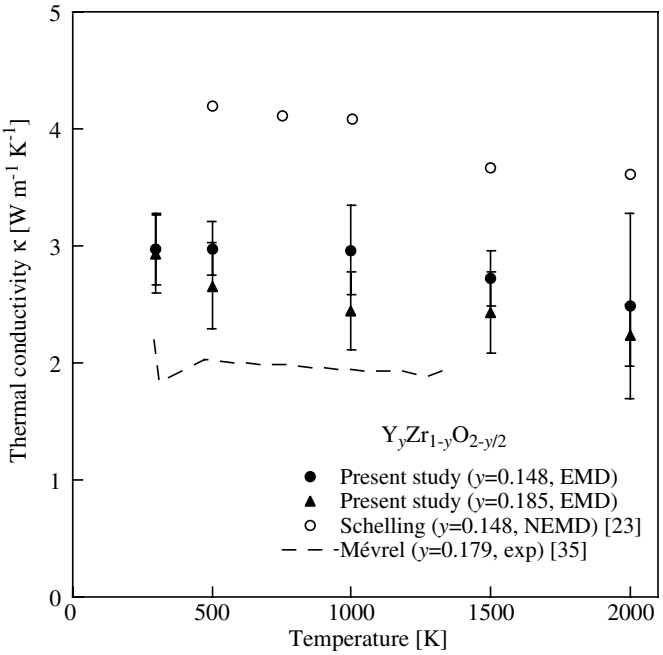

Fig. 4. Thermal conductivity of ZrO_2–Y_2O_3 system as a function of temperature. In the present study, Eq. (5) gives the thermal conductivity for EMD simulation.

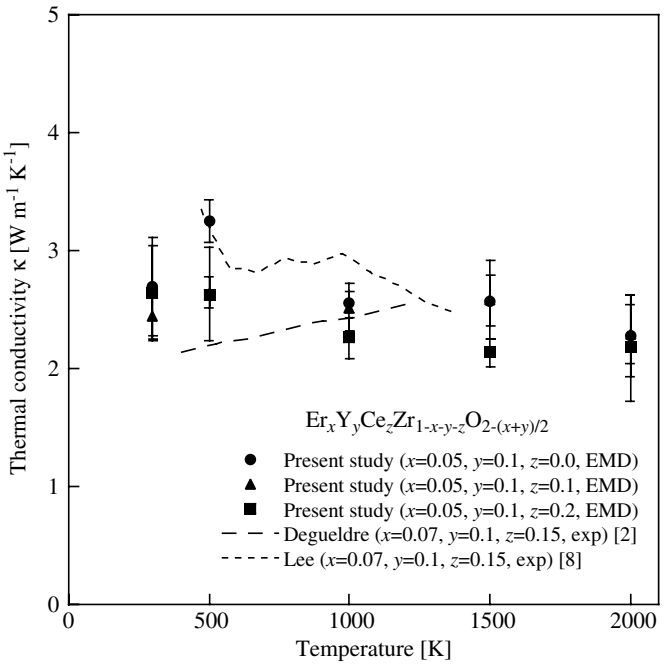

Fig. 5. Thermal conductivity of Ce-doped zirconia as a function of temperature.

dominates a lowering of thermal conductivity at low temperatures. The thermal conductivity of Pu-doped zirconia seems to be smaller than that of Ce-doped, although there is little difference between them. Rather than the difference in the kind of tetravalent ion, the MD study shows here that the increase in

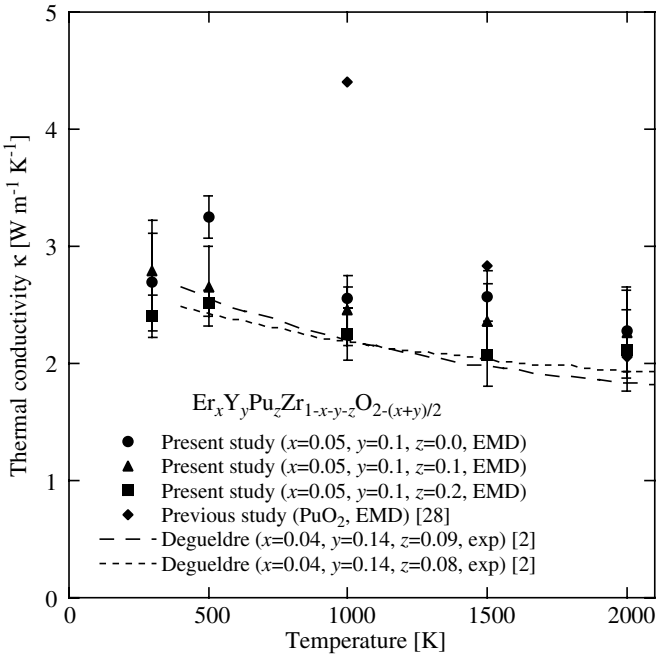

Fig. 6. Thermal conductivity of Pu-doped IMF as a function of temperature.

content of Pu (or Ce) diminishes slightly the thermal conductivity of zirconia-based IMF. It is caused by that such a heavy tetravalent metal as an impurity for the host material may be thermal resistant.

4. Conclusion

Thermal conductivities of $Er_xY_yM_zZr_{1-x-y-z}O_{2-(x+y)/2}$ (M = Ce or Pu) were calculated by MD simulations under equilibrium conditions from 300 to 2000 K. Born–Mayer–Huggins interatomic potentials with partially ionic model were used in the MD calculations. The thermal conductivities were formalized based on Green–Kubo theory and phenomenological equations in the present study. For $Y_yZr_{1-y}O_{2-y/2}$, it was shown that oxygen vacancies might be thermal resistant and that the thermal conductivity slightly decreased with increase of temperature. For $Er_xY_yM_zZr_{1-x-y-z}O_{2-(x+y)/2}$, the thermal conductivity decreased with increase of Ce or Pu content and was almost constant for temperature rather than inversely proportional to temperature. The thermal conductivity obtained by the EMD simulation for Pu-doped IMF is comparable with the experimental data. Change in the significance of the transport coefficients (i.e., thermal and ionic conductivities) was lowered by increasing the additive content. The cross-coupling effect of energy (or heat) and charge fluxes seemed to be strong at low z values and higher temperatures. In the future, the arrangement of rare-earth metals (i.e., Y and Er) will be taken into consideration because these may be related to the formation of defect cluster. In addition, the homogeneous NEMD calculation will be undertaken because its smooth implementation can be achieved for the EMD system.

Acknowledgements

The authors would like to thank K. Kawamura for the use of MXDORTO. The authors also thank S. Motoyama for advice concerning the calculation of the thermal conductivity.

References

[1] C. Degueldre, U. Kasemeyer, F. Botta, G. Ledergerber, Mat. Res. Soc. Symp. Proc. 412 (1995) 15.
[2] C. Degueldre, T. Arima, Y.W. Lee, J. Nucl. Mater. 319 (2003) 6.
[3] C. Degueldre, J.M. Paratte, J. Nucl. Mater. 274 (1999) 1.
[4] M.A. Pouchon, C. Degueldre, P. Tissot, Thermochim. Acta 323 (1998) 109.
[5] C. Degueldre, S. Conradson, Appl. Phys. A 73 (2001) 489.
[6] M. Burghartz, G. Ledergerber, F. Ingold, P. Heimgartner, C. Degueldre, Prog. Nucl. Energy 38 (2001) 247.

[7] C. Degueldre, P. Tissot, H. Lartigue, M. Pouchon, Thermochim. Acta 403 (2003) 267.
[8] Y.W. Lee, S.C. Lee, H.S. Kim, C.Y. Joung, C. Degueldre, J. Nucl. Mater. 319 (2003) 15.
[9] T. Arima, S. Yamasaki, S. Torikai, K. Idemitsu, Y. Inagaki, C. Degueldre, J. Alloys Compd. 398 (2005) 296.
[10] K. Yamada, K. Kurosaki, M. Uno, S. Yamanaka, J. Alloys Compd. 307 (2000) 1.
[11] K. Yamada, K. Kurosaki, M. Uno, S. Yamanaka, J. Alloys Compd. 307 (2000) 10.
[12] K. Kurosaki, K. Yamada, M. Uno, S. Yamanaka, K. Yamamoto, T. Namekawa, J. Nucl. Mater. 294 (2001) 160.
[13] P.J.D. Lindan, M.J. Gillan, J. Phys.: Condens. Matter 3 (1991) 3929.
[14] S. Motoyama, Y. Ichikawa, Y. Hiwatari, A. Oe, Phys. Rev. B 60 (1999) 292.
[15] A. Dwivedi, A.N. Cormack, Philos. Mag. A 61 (1990) 1.
[16] F. Shimojo, T. Okabe, F. Tachibana, M. Kobayashi, H. Okazaki, J. Phys. Soc. Jpn. 61 (1992) 2848.
[17] F. Shimojo, H. Okazaki, J. Phys. Soc. Jpn. 61 (1992) 4106.
[18] H.W. Brinkman, W.J. Briels, H. Verweij, Chem. Phys. Lett. 247 (1995) 386.
[19] X. Li, B. Hafskjold, J. Phys.: Condens. Matter 7 (1995) 1255.
[20] T. Tojo, H. Kawaji, T. Atake, Solid State Ion. 118 (1999) 349.
[21] Y. Yamamura, S. Kawasaki, H. Sakai, Solid State Ion. 126 (1999) 181.
[22] N. Sawaguchi, H. Ogawa, Solid State Ion. 128 (2000) 183.
[23] P.K. Schelling, S.R. Phillpot, J. Am. Ceram. Soc. 84 (2001) 2997.
[24] T. Arima, K. Fukuyo, K. Idemitsu, Y. Inagaki, J. Mol. Liq. 113 (2004) 67.
[25] K. Hirao, K. Kawamura, Material design using personal computer, Shokabo, Tokyo, 1994.
[26] H. Inaba, R. Sagawa, H. Hayashi, K. Kawamura, Solid State Ion. 122 (1999) 95.
[27] H. Hayashi, R. Sagawa, H. Inaba, K. Kawamura, Solid State Ion. 131 (2000) 281.
[28] T. Arima, S. Yamasaki, Y. Inagaki, K. Idemitsu, J. Alloys Compd. 400 (2005) 43.
[29] G.V. Lewis, C.R.A. Catlow, J. Phys. C 18 (1985) 1149.
[30] B. Bernu, J.P. Hansen, Phys. Rev. Lett. 48 (1982) 1375.
[31] C. Pierleoni, G. Ciccotti, J. Phys.: Condens. Matter 2 (1990) 1315.
[32] P. Sindzingre, M.J. Gillan, J. Phys.: Condens. Matter 2 (1990) 7033.
[33] N. Galamba, C.A. Nieto de Castro, J.F. Ely, J. Chem. Phys. 120 (2004) 8676.
[34] C. Pierleoni, G. Ciccotti, B. Bernu, Europhys. Lett. 4 (1987) 1115.
[35] K. Idemitsu, T. Arima, Y. Inagaki, S. Torikai, M.A. Pouchon, J. Nucl. Mater. 319 (2003) 31.
[36] R. Mévrel, J.C. Laizet, A. Azzopardi, B. Leclercq, M. Poulain, O. Lavigne, D. Demange, J. Euro. Ceram. Soc. 24 (2004) 3081.
[37] S. Raghavan, H. Wang, R.B. Dinwiddie, W.D. Porter, M.J. Mayo, Scripta Mat. 39 (1998) 1119.